

Stochastic reconstruction of sandstones

C. Manwart,¹ S. Torquato,² and R. Hilfer^{1,3}

¹*Institut für Computeranwendungen 1, Universität Stuttgart, 70569 Stuttgart, Germany*

²*Department of Chemistry and Princeton Materials Institute, Princeton University, Princeton, New Jersey 08544*

³*Institut für Physik, Universität Mainz, 55099 Mainz, Germany*

(Received 4 February 2000)

A simulated annealing algorithm is employed to generate a stochastic model for a Berea sandstone and a Fontainebleau sandstone, with each a prescribed two-point probability function, lineal-path function, and “pore size” distribution function, respectively. We find that the temperature decrease of the annealing has to be rather quick to yield isotropic and percolating configurations. A comparison of simple morphological quantities indicates good agreement between the reconstructions and the original sandstones. Also, the mean survival time of a random walker in the pore space is reproduced with good accuracy. However, a more detailed investigation by means of local porosity theory shows that there may be significant differences of the geometrical connectivity between the reconstructed and the experimental samples.

PACS number(s): 61.43.Gt

I. INTRODUCTION

The microstructures of porous media determine their macroscopic physical properties [1–3], such as conductivity, elastic constants, relaxation times, permeabilities, or thermal properties. The relation between geometric microstructure and physical properties is a fundamental open problem whose solution is important to many applications ranging from geophysics to polymer physics and material science. For the geometric modeling of porous media, it is therefore important to characterize microstructures quantitatively and to construct models using given geometric characteristics.

The reconstruction of random media with given stochastic properties is also of great interest for a variety of other reasons:

(i) Digitized three-dimensional geometries of real sandstones are difficult to obtain. Therefore the reconstruction provides a method for easily generating detailed geometries as needed, e.g., in numerical calculations of macroscopic material parameters like those mentioned above.

(ii) The reconstruction of three-dimensional samples from two-dimensional data.

(iii) Any calculation of macroscopic quantities of random media needs a set of stochastic functions that describes the geometry. The reconstruction can help to decide which functions one should use. The present work will focus mainly on the latter question, the so-called inverse problem.

Recently, a simulated annealing algorithm for the reconstruction of random porous media with predefined stochastic functions was proposed [4]. This method was used for the reconstruction of two-phase porous media, i.e., sandstones, with a given two-point probability function and a lineal-path function, which were measured from real sandstones [5,6]. In the present article, we will continue this work. An advantage of the simulated annealing is that it allows for the reconstruction of a variety of different stochastic functions with the available CPU time being the only limit on the use of a set of functions. In Refs. [5], [6], the two-point probability function and the lineal-path function were used. Here we will extend the investigations to the reconstruction of the so-called

“pore size” distribution [7,8], which is not the usual quantity obtained from mercury porosimetry. We will study a Berea sandstone and a Fontainebleau sandstone.

A comparison of the reconstructions with the original sandstones shows to what extent the characteristics of the original geometry are reconstructed. A salient feature of the original sandstone is the high degree of connectivity of the pore space. Hence one important criterion for judging a stochastic reconstruction method is its ability to reproduce the connectivity of the original sandstone. It is shown that Berea reconstruction does a better job of capturing connectivity than does the Fontainebleau reconstruction, although neither captures connectivity particularly well. Another important criterion is the ability of the reconstruction procedure to reproduce the macroscopic properties of the original materials. We show that the mean survival times of our reconstructions of both sandstones agree well with mean survival times of the original sandstones.

The paper is organized as follows. In Sec. II we describe the reconstruction algorithm. In Sec. III we introduce the quantities we use in the reconstruction process and to characterize the sandstones. Because detailed discussions can be found in the references, we will focus mainly on practical aspects and details of the implementation. In Sec. IV we present the results for the reconstructions of a Berea sandstone and a Fontainebleau sandstone, respectively.

II. THE RECONSTRUCTION METHOD

A two-phase porous medium consists of a pore or void phase \mathbb{P} and a matrix or rock phase \mathbb{M} . Its microgeometry is described in detail by the characteristic function

$$\chi(\vec{x}) = \begin{cases} 0 & \text{for } \vec{x} \in \mathbb{M}, \\ 1 & \text{for } \vec{x} \in \mathbb{P}. \end{cases} \quad (1)$$

For a discretized sample, $\vec{x} = (j_1 a, j_2 a, j_3 a)$ is the position vector of a cubic grid with $j_i = 0, \dots, M_i - 1$, lattice constant a ,

and size $M_1 \times M_2 \times M_3$. The total number of grid points is given by $N = M_1 M_2 M_3$. In the following we will also refer to a grid point as a voxel.

The porosity ϕ , the probability of finding a point in pore space, is given by

$$\phi = \langle \chi(\vec{x}) \rangle. \quad (2)$$

With the assumption of a homogeneous, stationary, and ergodic stochastic porous medium, the angular brackets denote a volume average.

The reconstruction is carried out by means of a simulated annealing method [4] with the target or ‘‘energy’’ function defined as

$$E_t(f_t) = \sum_{\vec{x}} |f_t(\vec{x}) - f_{\text{ref}}(\vec{x})|^2. \quad (3)$$

The function f_{ref} is the stochastic function to be reconstructed, whereas f_t is the actual value of this function measured at iteration step t . For the reconstruction of more than one function, the energy E_t at the iteration step t is given by $E_t = \sum_k E_t(f_t^{(k)})$, where the index k numbers the different functions to be reconstructed.

Starting from a random configuration with porosity ϕ , two voxels of different phases are exchanged at each iteration step. Thus the porosity ϕ remains constant during the reconstruction process. The new configuration is accepted with the probability given by the Metropolis rule

$$P = \begin{cases} 1 & \text{if } E_t \leq E_{t-1}, \\ e^{(E_{t-1} - E_t)/T} & \text{if } E_t > E_{t-1}, \end{cases} \quad (4)$$

where T plays the role of a temperature. In the case of rejection, the old configuration is restored. By decreasing the temperature T , configurations with minimal energy E , i.e., with minimal deviations of the stochastic functions $f_t^{(k)}$ from their reference functions $f_{\text{ref}}^{(k)}$, are generated. The process terminates after a certain number of consecutive rejections. Here the reconstruction was finished after 10^5 consecutive rejections.

III. MEASURED QUANTITIES

A. The two-point probability function

Using Eq. (1), the two-point probability function is defined as

$$\mathbf{S}_2(\vec{x}_1, \vec{x}_2) = \langle \chi(\vec{x}_1) \chi(\vec{x}_2) \rangle. \quad (5)$$

For a homogeneous and isotropic medium, $\mathbf{S}_2(\vec{x}_1, \vec{x}_2) = \mathbf{S}_2(r)$ with $r = |\vec{x}_1 - \vec{x}_2|$. In this case $\mathbf{S}_2(r)$ can be evaluated without loss of information from the intersection of the sample with a plane or even a line. To speed up the numerical evaluation of \mathbf{S}_2 it is therefore sufficient to sample \mathbf{S}_2 only in directions of the principal axis given by the unit vectors \vec{e}_i [4].

Hence \mathbf{S}_2 is calculated by evaluating Eq. (5) for every pair of voxels at \vec{x}_1 and $\vec{x}_2 = \vec{x}_1 + r\vec{e}_i$ with $r = 0, 1, \dots, r_c$ where r_c is a cutoff value determined by the system size or a multiple of the correlation length. During the reconstruction only

those terms in \mathbf{S}_2 are updated that have changed due to the exchange of voxels. On the sample boundaries we impose periodic boundary conditions.

For reconstruction purposes, this simplification, i.e., the reconstruction of \mathbf{S}_2 only in the direction of the three coordinate axes, may create some problems. Because all other directions remain unoptimized, \mathbf{S}_2 measured in these directions may differ from the reference function. If this happens the reconstructed sample is no longer isotropic [9,10]. Furthermore, the reconstruction of \mathbf{S}_2 only along orthogonal lines reduces the three-dimensional optimization problem effectively to the optimization of three one-dimensional two-point probability functions. This may reduce the number of conditions that the two-point probability function has to fulfill to be realizable [11], and may lead one to conclude incorrectly that the reconstruction is realizable in the space dimension of interest. However, the problem of realizability does not apply to the reconstructions presented here, because the two-point probability functions used as reference functions are measured from digitized three-dimensional images of real sandstones. Nevertheless, the reconstructions have to be checked for their isotropy.

The isotropy of the reconstructions can be improved, e.g., by a full reconstruction of the two-point probability function using Fourier transform techniques or by rotating the sample during the reconstruction. This was done for two-dimensional reconstructions in [10]. However, for three-dimensional reconstructions this leads to a prohibitive increase of computation time.

For the specific surface s , i.e., the surface per unit volume of the interface between pore space and matrix space, it is known that [12]

$$s = -4 \left. \frac{\partial \mathbf{S}_2(r)}{\partial r} \right|_{r=0}. \quad (6)$$

Therefore a reconstruction of \mathbf{S}_2 implies that the specific surface area of the reconstructions matches that of the reference sample. Equation (6) may also be used for the calculation of the specific surface. Here we use a different, numerically very efficient method introduced in [13] for calculating s .

B. Lineal-path function and ‘‘pore size’’ distribution

The lineal-path function $L(r)$ is defined as the probability of finding a line segment of length r entirely in pore space when the line segment is randomly thrown into the porous medium [14]. Hence for $r=0$, $L(0) = \phi$ holds. The lineal-path function is related to the linear contact distribution introduced in mathematical stochastic geometry [15–17]. The lineal-path function is calculated as follows: For a given pore voxel, the lineal path r in units of the resolution a is given as the number of pore voxels lying between the given pore voxel and the nearest matrix voxel in direction \vec{e}_i . Evaluating the line segments starting from each pore voxel in all three coordinate directions \vec{e}_i and counting the number $l(r)$ of line segments with length r , the lineal-path function is given by

$$L(r) = l(r) / [(M_1 - r)M_2M_3 + M_1(M_2 - r)M_3 + M_1M_2(M_3 - r)], \quad (7)$$

where we assume nonperiodic boundary conditions.

The lineal-path function incorporates information about the connectivity of the pore space. Of course it would be desirable to reconstruct functions that provide more complete information about the geometric connectivity of the pore space, as for example the cluster correlation function [3] or the local percolation probability [2], but currently the computation time for evaluating these functions prevents their use in the above reconstruction scheme.

The ‘‘pore size’’ distribution function $P(\delta)$ is defined such that $P(\delta)d\delta$ is the probability that a randomly chosen point in the pore space lies at a distance $[\delta, \delta + d\delta]$ from the nearest point on the interface [7,8]. It is related to the spherical contact distribution [15,16,18]. The associated cumulative distribution function

$$F(\delta_o) = \int_{\delta_o}^{\infty} P(\delta)d\delta \quad (8)$$

gives the fraction of the pore space that has a diameter larger than δ_o . Clearly

$$P(\delta) = -\frac{\partial F}{\partial \delta}, \quad (9)$$

and

$$P(0) = \frac{s}{\phi}. \quad (10)$$

The mean pore size is given as

$$\langle \delta \rangle = \int_0^{\infty} \delta P(\delta)d\delta = \int_0^{\infty} F(\delta)d\delta. \quad (11)$$

The quantity $P(\delta)$ arises in rigorous bounds on the mean survival time [8].

We compute an approximation to $P(\delta)$ by choosing a random point in pore space and measuring its distance δ to the nearest point on the matrix-pore interface assuming periodic boundary conditions. This process is repeated for several random points in pore space. The ‘‘pore size’’ distribution is then obtained by binning the distances δ and dividing by the number of random placements in pore space. We emphasize that the random placements in pore space are not necessarily grid points. The computation of δ is only approximate because it requires a modeling of the interface between pore and matrix space. Here, we assume that the internal surface is given by the surface of the cubic voxels. This is the same modeling that is used, e.g., in a computation of the mean survival time or in finite difference calculations of transport properties. In general, this may overestimate the specific surface area appearing in Eq. (10) by a factor of roughly 1.5 [19]. For use in the reconstruction we measured δ as the distance between a pore voxel and the nearest matrix voxel. The resulting function is not equal to $P(\delta)$ because δ can now only take values of $\delta = \sqrt{i^2 + j^2 + k^2}$ with $i, j, k \in \mathbb{Z}$.

C. The total fraction of percolating cells

The total fraction of percolating cells p is a key measure in local porosity theory [20,2]. Local porosity theory measures the fluctuations of morphological quantities, e.g., porosity, specific surface, and connectivity, in cubic subsamples of the total sample [21]. We will refer to such a cubic subsample with side length L as a measurement cell. Based on the scale-dependent morphological quantities, the theory provides scale-dependent estimates for transport parameters from a generalized effective medium theory [22,23].

Let $\mu(\phi, L)d\phi$ be the probability that a given measurement cell of side length L has a porosity in the interval $[\phi, \phi + d\phi]$. The probability density function μ is called local porosity distribution. The probability that a given measurement cell with porosity ϕ is percolating in all three directions is the local percolation probability function $\lambda(\phi, L)$. Here percolating in all three directions means that each face of the measurement cell is connected to the opposite face with a path lying entirely in pore space. Using this, the total fraction of percolating cells is given by

$$p(L) = \int_0^1 \mu(\phi, L)\lambda(\phi, L)d\phi. \quad (12)$$

The total fraction of percolating cells $p(L)$ is the probability of finding a measurement cell with side length L , which is percolating in all three directions. Hence p is a measure for the geometrical connectivity.

D. The mean survival time

In contrast to the previous quantities, the mean survival time τ is not a purely geometrical but a physical observable. The mean survival time τ is the average lifetime of a random walker, which can freely move in pore space, but gets instantly absorbed on contact with the pore-matrix interface. It is a measure of a characteristic pore size. The mean survival time τ is calculated using a first passage cube (FPC) algorithm [19,24]. The FPC algorithm uses the fact that the mean time it takes for a certain type of diffusive random walker starting at the center of a cube with side length $2L$ to cross the surface of this cube is given by

$$\tau(T) \approx 0.22485L^2. \quad (13)$$

Hence it is not necessary to simulate the steps of the walker in detail. Instead, one determines the biggest cube centered around the position of the walker, which is still entirely in pore space. The walker then jumps on the surface of this FPC and a time given by Eq. (13) is added to its lifetime. This procedure is iterated until the walker touches the interface and gets absorbed. The mean survival time is given by averaging over many walkers.

The probability with which the walker jumps to a certain point on the surface of the FPC is described by a probability density function $w(y, z)$ where y and z are the coordinates on the surface, assuming without loss of generality that $x = \pm L$. For an analytic expression of $w(y, z)$ we refer to [24].

TABLE I. Characteristic quantities of the Berea sandstone, its LS reconstructions, and its PS reconstructions. The values given for the reconstructions are averaged over five configurations.

	Berea	LS	PS
Porosity	0.1775	0.1775	0.1775
Specific surface (mm^{-1})	13.9	14.7	14.4
Mean survival time τD (μm^2)	100	89	93
Mean pore size $\langle \delta \rangle$ (μm)	6.71	6.52	6.66
f_p (%)	97.16	88.76	85.49
$p(L=60)$	0.997	0.747	0.712

IV. RESULTS

In this section we present results for reconstructions of a Berea sandstone and a Fontainebleau sandstone. For both sandstones we computed reconstructions with the lineal-path function and the two-point probability function (LS reconstruction) as well as reconstructions with the ‘‘pore size’’ distribution function and the two-point probability function (PS reconstruction). The Berea sandstone and its reconstructions have the dimension $128 \times 128 \times 128$ and the resolution $a = 10 \mu\text{m}$. The porosity is $\phi = 0.1775$. The Fontainebleau sandstone has dimensions $299 \times 300 \times 300$ and its reconstructions have the dimension $128 \times 128 \times 128$. The resolution is $a = 7.5 \mu\text{m}$; the porosity is $\phi = 0.1355$. The reconstructed functions were calculated as described above; i.e., we used periodic boundary conditions for all except for the lineal-path function. The two-point probability function $S_2(r)$ was reconstructed in the interval $r = 0, 1, \dots, 63$. The annealing process terminated after 10^5 subsequent rejections.

We performed five LS reconstructions and five PS reconstructions for both the Berea and the Fontainebleau sandstones. Some of the results are summarized in Table I for the Berea sandstone and in Table II for the Fontainebleau sandstone, respectively. The values are averaged over five reconstructions. The quantity τD is the mean survival time multiplied by the diffusion coefficient D for the random-walk process discussed above. The quantity f_p gives the fraction of pore voxels that belong to the percolating cluster.

Figure 1 shows two-dimensional slices of the original and the reconstructed sandstones. The top row shows the original sandstones, the row in the middle the LS reconstructions, and the bottom row the PS reconstructions. The slices were taken from reconstructions with the value of $p(L=60)$, which is close to the average values given in the tables. All slices are chosen to have average porosity. In the case of the

TABLE II. Characteristic quantities of the Fontainebleau sandstone, its LS reconstructions, and its PS reconstructions. The values given for the reconstructions are averaged over five configurations.

	Fontainebleau	LS	PS
Porosity	0.1355	0.1355	0.1355
Specific surface (mm^{-1})	10.0	10.6	10.4
Mean survival time τD (μm^2)	134	129	121
Mean pore size $[\delta]$ (μm)	7.85	7.88	7.73
f_p (%)	99.35	52.22	51.26
$p(L=60)$	0.956	0.265	0.234

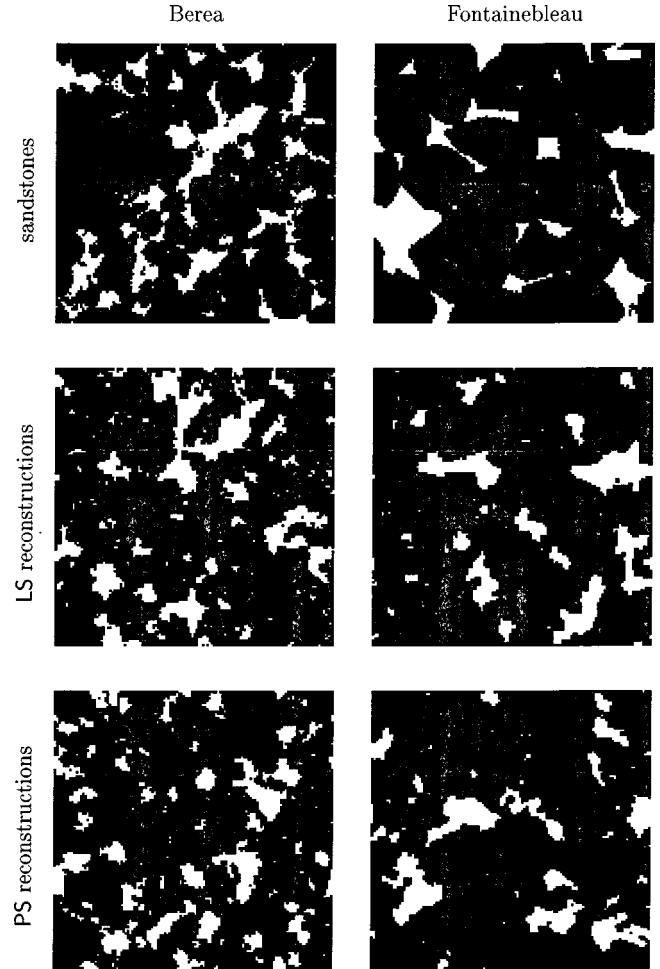


FIG. 1. Two-dimensional slices of the Berea sandstone, the Fontainebleau sandstone, and two reconstructions of each. The top row shows the original sandstones, the middle row the LS reconstructions, and the bottom row the PS reconstructions with the Berea sandstones on the left and the Fontainebleau sandstones on the right. All slices have approximately the average porosity of $\phi = 0.1775$ for the Berea and $\phi = 0.1355$ for the Fontainebleau, respectively.

Berea sandstone, the reconstructions look similar to the original sandstone, while for the Fontainebleau sandstone the reconstructions are clearly distinguishable from the original sandstone. The matrix of the original Fontainebleau sandstone shows a granular structure where single grains can be identified. The pores between these grains are long and narrow. In the reconstructions, no granular structure of the matrix space is visible. The pores of the reconstructions are more rounded in shape. For both sandstones, the number of isolated pores is significantly higher in the reconstructions. This is expressed by f_p , the fraction of pore space belonging to the percolating cluster. For the Berea, 97.16% of the pore space belongs to the percolating cluster whereas for the reconstructions this fraction is roughly 10% smaller. For the Fontainebleau the difference is even bigger. In the original sandstone, 99.35% of the pore space percolates while for the reconstructions f_p is approximately 52%. Here we find that one LS and PS reconstruction of the Fontainebleau are not percolating in all three directions.

In the course of our work we also used a slowly decreas-

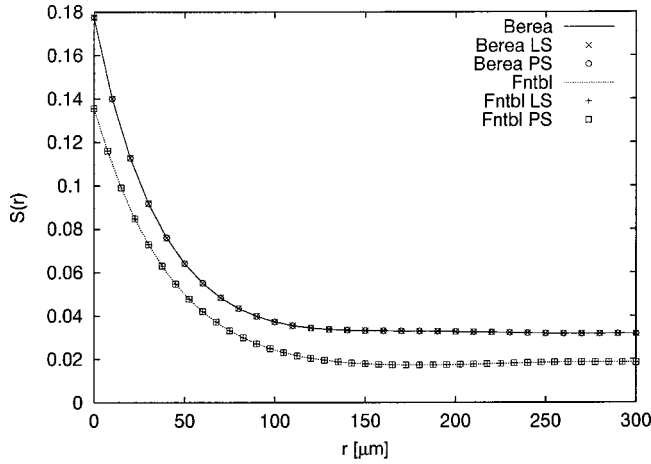


FIG. 2. Two-point probability functions S_2 of the Berea (top) and the Fontainebleau (bottom) sandstones. The solid lines show the reference functions, the points show typical reconstructed functions for a LS and a PS reconstruction.

ing step function for the temperature T to obtain an optimal match of the reconstructed functions. Surprisingly, with a slow cooling schedule the majority of the reconstructed configurations was not percolating in all three directions. Furthermore, the reconstructed samples showed a strong anisotropy with $E(\tilde{S}_2)$ of the order 10^{-2} , where \tilde{S}_2 denotes the two-point probability function measured in the directions $e_i + e_{j \neq i}$.

For the reconstructions presented here, we used a fast exponential cooling schedule $T = \exp(t/10^5)$ where t as above denotes the iteration step. This cooling schedule took approximately $30N$ iterations steps to complete a reconstruction, whereas the slow cooling took more than $300N$ iterations steps. Using the fast cooling schedule all reconstructions of the Berea sandstone are percolating in all three directions and only one LS and one PS reconstruction of the Fontainebleau are not percolating. Also, with the fast cooling schedule the reconstructed functions are matched very well; i.e., $E(S_2)$ is of the order 10^{-10} , $E(L)$ is of the order 10^{-8} . Moreover, the anisotropy measured in terms of $E(\tilde{S}_2)$ was reduced by an order of magnitude. Plotting \tilde{S}_2 , only the PS reconstructions of the Fontainebleau showed small deviations.

Our explanation for the fact that a slower cooling schedule results in reconstructions with stronger anisotropy and only poor connectivity is the artificial anisotropy introduced by reconstructing S_2 and L only in three directions. With an increasing number of iterations the influence of the isotropic, random starting configuration is decreased while the anisotropic calculation scheme of the two-point probability functions as described above becomes more significant. This view agrees with previous work [5,6] where three-dimensional isotropic reconstructions of sandstones also using a fast cooling schedule were presented. The poor connectivity of the reconstructions with a slow cooling schedule may be a result of their strong anisotropy.

In Figs. 2, 3, and 4 the two-point probability functions S_2 , the lineal-path functions L , and the ‘‘pore size’’ distribution functions P , respectively, are plotted for both sandstones using lines and for typical reconstructions using dots.

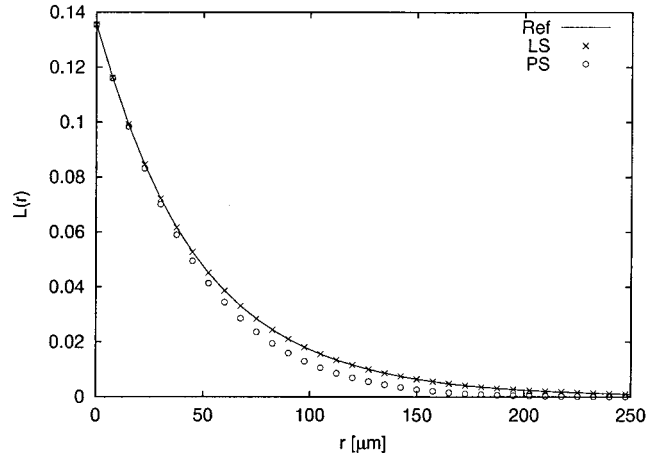
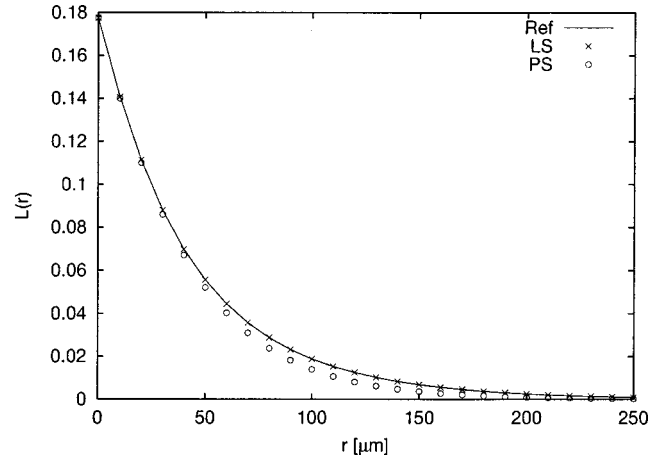


FIG. 3. Lineal-path functions L of the Berea (top) and the Fontainebleau (bottom) sandstone. The solid lines correspond to the reference functions, the points show typical LS and typical PS reconstructions.

Here typical means that the energy given by Eq. (3) of the reconstructed functions is close to the average value. In the case of the two-point probability function, the reconstructed functions appear to be indistinguishable from the reference functions. The same applies to the lineal-path functions measured from the LS reconstructions. The lineal-path functions of the PS reconstructions clearly underestimate the reference functions. Complementary to this, P is equally matched by both types of reconstructions as shown in Fig. 4. A logarithmic plot of P and L reveals that the reconstructions only poorly match the tails of those functions. This is due to the extremely small values of $P(\delta)$ and $L(r)$ for large δ and large r , respectively. Furthermore, for the lineal-path function L this may be a finite size effect because L is a long ranged function with $L(r) > 0$ for values of r in the order of a third of the system size.

Looking at Fig. 4 it seems that for our reconstructions the lineal-path function L and the two-point probability function S_2 incorporate nearly the same information about the shape of the pores as S_2 and P do. Moreover, as seen from Fig. 3 the PS reconstruction lacks information about long line segments. This may be understood from the fact that P is a very short ranged function with $P(\delta) \neq 0$ only in a range smaller than the correlation length. For the Berea sandstone $P(\delta) = 0$ for $\delta > 60 \mu\text{m}$, and for the Fontainebleau sandstone

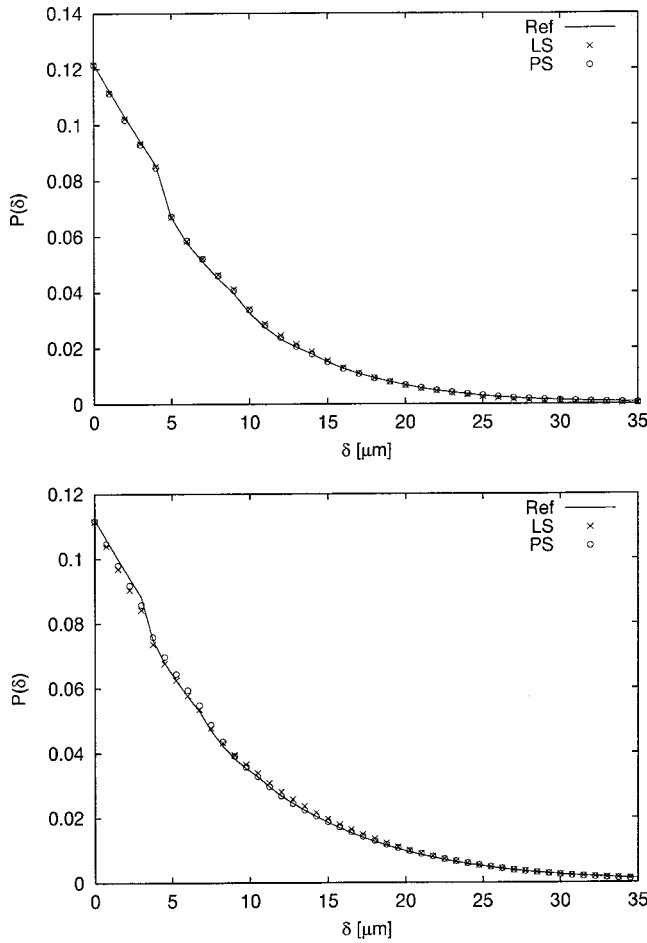


FIG. 4. ‘‘Pore size’’ distribution functions P of the Berea sandstone (top) and the Fontainebleau sandstone (bottom). The solid lines correspond to the reference functions, the points show typical LS and typical PS reconstructions.

$P(\delta)=0$ for $\delta>78\ \mu\text{m}$. Hence even though P contains full three-dimensional information about spherical regions in pore space, similar information is already provided by the two-point probability function S_2 .

Looking at the parameters given in Tables I and II, the PS reconstructions match the specific surface better. This is expected because the specific surface s can be measured from either S_2 or P as seen from Eqs. (6) and (10). However, the value of s measured from Eq. (10) turns out to be roughly a factor of 1.5 bigger than the value computed from Eq. (6). This is due to the simple surface modeling in the calculation of P as discussed above. We believe the kink in $P(\delta)$ for $\delta=0.5a$ to be an artifact of the discretization.

In the case of Berea we find the best agreement of the mean pore size $\langle\delta\rangle$ for the PS reconstructions, while in the case of the Fontainebleau the match appears to be better for the LS reconstruction. The lineal-path function seems to be better suited to describe the long narrow pores of the Fontainebleau sandstone than the ‘‘pore size’’ distribution. As already seen from the two-dimensional slices, the appearance of the Berea sandstone is quite similar to the appearance of the reconstructions. The pores are much more rounded in shape. Here the reconstruction is slightly improved with respect to the mean pore size by incorporating P , which contains information about spherical regions.

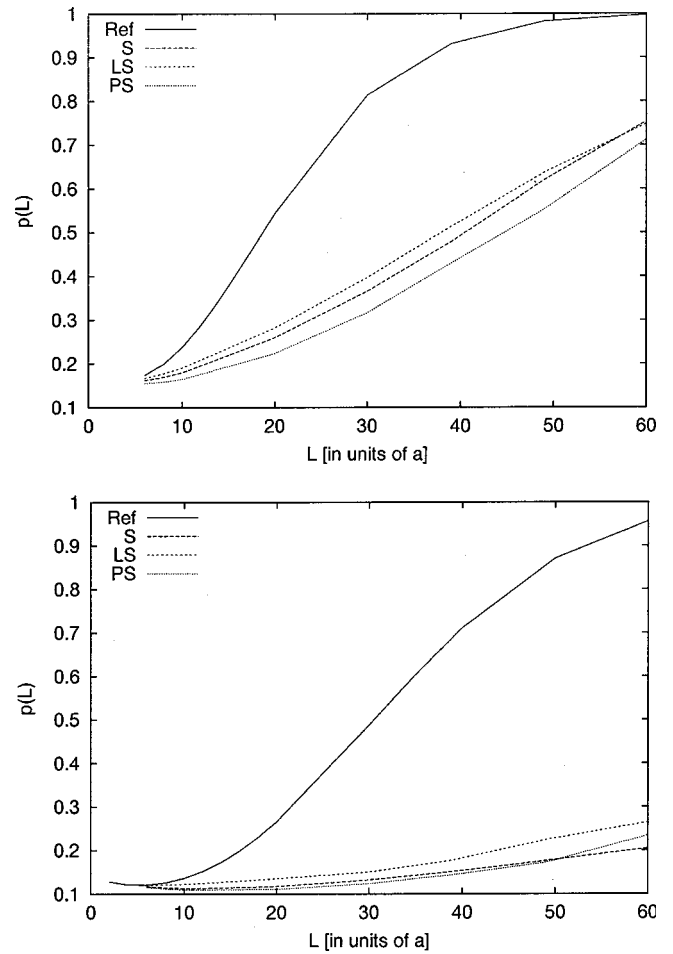


FIG. 5. Total fraction of percolating cells p for the Berea sandstone (top) and the Fontainebleau sandstone (bottom). The solid lines show p measured from the original sandstones. The curves shown for the reconstructions are averaged over five configurations each.

We find analogous results for the mean survival time τ , which is a diffusive transport property. In fact, the mean survival time can be related to the mean pore size [8]. The mean survival time is a physical transport property, but unlike the fluid permeability, it does not capture the same information about the dynamical connectivity of the pore space; indeed, neither does the conductivity (or formation factor) [8,25]. Nonetheless, a cross-property formula relating the fluid permeability to a combination of the porosity, mean survival time, and formation factor F has been shown to be a highly accurate estimate of k for sandstones [26]. This cross-property formula was used to demonstrate that the permeability of another reconstructed sandstone [5] was in excellent agreement with the exact Stokes solution determination of the permeability of the original sandstone [26].

We note that a good match of τ alone may not always indicate a good match for \mathcal{F} or k . In fact, combining results from [22,23,6] suggests that \mathcal{F} correlates strongly with the local percolation probability p , which is a measure of the geometrical connectivity. We find significant differences between the local percolation probabilities of the real sandstones and the present reconstructions.

Figure 5 shows plots of the local percolation probability p for the original sandstones, the LS reconstructions, the PS

reconstructions, and reconstructions of the two-point probability function only (\mathbf{S} reconstruction). The pure \mathbf{S} reconstructions are included here for comparison to previous work [6]. The curves shown for the reconstructions are averaged over five configurations each. The local percolation probability p of the reconstructions lies well below the curves of the original sandstones. From this plot it seems that neither the use of \mathbf{L} nor the use of \mathbf{P} can significantly improve the geometric connectivity compared to the reconstruction of \mathbf{S}_2 only. The differences between the curves of the three reconstructions seem to be within the range of statistical fluctuations. Nevertheless, a similar result for the \mathbf{S} reconstruction of the Fontainebleau sandstone was presented in [6] for a larger sample. Other work [5] showed that a \mathbf{LS} reconstruction of a different Fontainebleau sandstone reproduced the geometric connectivity well.

In general, when comparing the \mathbf{LS} reconstructions and the \mathbf{PS} reconstructions the resulting configurations are quite similar. For our reconstructions, the two-point probability function \mathbf{S}_2 and the lineal-path function \mathbf{L} incorporate nearly the same morphological information as \mathbf{S}_2 and \mathbf{P} do. Looking at the reconstructions of the Berea sandstone and the reconstructions of the Fontainebleau sandstone it appears that the latter one is much more demanding to reconstruct. This may be due to its characteristic granular structure, the narrow pore throats, the lower porosity, and to the larger sample size of the original sandstone. We also note that the

Berea sample is only $128 \times 128 \times 128$, resulting in poor statistical quality.

Our work has shown that simulated annealing provides a flexible and simple to implement method for reconstructing two-phase random media and that local porosity theory provides highly sensitive tools for their comparison and analysis. However, with the present computer power there is still a need to introduce simplifications to reduce the computation time. Reconstructing the two-point probability function \mathbf{S}_2 only in certain directions may artificially introduce a strong anisotropy or affect the connectivity. We find that a fast cooling schedule can reduce this problem. This implies that the final configuration is not completely independent from the initial configuration, and hence the reconstructed microstructure does not only depend on the reconstructed statistical functions, which would be desirable.

ACKNOWLEDGMENTS

C.M. thanks the Princeton Materials Institute at Princeton University for their hospitality and C. Yeong for helpful discussions. C.M. and R.H. gratefully acknowledge financial support by the Deutsche Forschungsgemeinschaft and the Deutscher Akademischer Austauschdienst. S.T. was supported by the Engineering Research Program of the Office of Basic Energy Sciences at the U.S. Department of Energy under Grant No. DE-FG02-92ER14275.

-
- [1] M. Sahimi, *Flow and Transport in Porous Media and Fractured Rock* (VCH Verlagsgesellschaft mbH, Weinheim, 1995).
- [2] R. Hilfer, *Adv. Chem. Phys.* **XCII**, 299 (1996).
- [3] S. Torquato, *Appl. Mech. Rev.* **44**, 37 (1991).
- [4] C. L. Y. Yeong and S. Torquato, *Phys. Rev. E* **57**, 495 (1998).
- [5] C. L. Y. Yeong and S. Torquato, *Phys. Rev. E* **58**, 224 (1998).
- [6] B. Biswal *et al.*, *Physica A* **273**, 452 (1999).
- [7] A. Scheidegger, *The Physics of Flow Through Porous Media* (University of Toronto Press, Toronto, 1974).
- [8] S. Torquato and M. Avellaneda, *J. Chem. Phys.* **95**, 6477 (1991).
- [9] C. Manwart and R. Hilfer, *Phys. Rev. E* **59**, 5596 (1999).
- [10] D. Cule and S. Torquato, *J. Appl. Phys.* **86**, 3428 (1999).
- [11] S. Torquato, *J. Chem. Phys.* **111**, 1 (1999).
- [12] P. Debye, H. Anderson, and H. Brumberger, *J. Appl. Phys.* **28**, 679 (1957).
- [13] C. Lang, J. Ohser, and R. Hilfer, *J. Pattern Recognition* (to be published).
- [14] B. Lu and S. Torquato, *Phys. Rev. A* **45**, 922 (1992).
- [15] P. Delfiner, *J. Microsc.* **95**, 203 (1972).
- [16] D. Stoyan, W. Kendall, and J. Mecke, *Stochastic Geometry and its Applications* (Wiley, New York, 1987).
- [17] The lineal-path function is related to the linear contact distribution function $H_l(r)$ as defined in [16] with a line segment as the structuring element \mathbf{B} by the formula $L(r) = \phi(1 - H_l(r))$. A general contact distribution with structuring element \mathbf{B} containing the origin may be defined as the probability distribution function of the random variable $R = \inf\{s: \mathbf{M} \cap s\mathbf{B} \neq \emptyset\}$ under the condition that $R > 0$.
- [18] We note that \mathbf{F} is the same as one minus the so-called contact distribution function H_S , $F(\delta) = 1 - H_S(\delta)$, with a sphere of radius δ as the structuring element \mathbf{B} [16].
- [19] D. A. Coker and S. Torquato, *J. Appl. Phys.* **77**, 955 (1995).
- [20] R. Hilfer, *Phys. Rev. B* **45**, 7115 (1992).
- [21] R. Hilfer, in *Räumliche Statistik und Statistische Physik*, edited by D. Stoyan and K. Mecke (Springer, Berlin, 2000).
- [22] J. Widjajakusuma, B. Biswal, and R. Hilfer, *Comput. Mater. Sci.* **16**, 70 (1999).
- [23] R. Hilfer, J. Widjajakusuma, and B. Biswal, *Granular Matter* (to be published).
- [24] S. Torquato, In Chan Kim, and D. Cule, *J. Appl. Phys.* **85**, 1560 (1999).
- [25] M. Avellaneda and S. Torquato, *Phys. Fluids A* **3**, 2529 (1991).
- [26] L. M. Schwartz, N. Martys, D. P. Bentz, E. J. Garboczi, and S. Torquato, *Phys. Rev. E* **48**, 4584 (1993).